Assessment of reusable graphene wool adsorbent for the simultaneous removal of selected 2-6 ringed polycyclic aromatic hydrocarbons from aqueous solution

Adedapo O. Adeola [a] and Patricia B.C. Forbes [a*]

[a]*Department of Chemistry, Faculty of Natural and Agricultural Sciences, University of Pretoria, Lynnwood Road, Hatfield, Pretoria 0002, South Africa.*

[*]*patricia.forbes@up.ac.za*

Abstract

The United States Environmental Protection Agency categorized polycyclic aromatic hydrocarbons (PAHs) as hazardous to humans upon acute and/or chronic exposure. This study investigated the simultaneous adsorption of several PAHs onto graphene wool (GW), thereby providing holistic insights into the competitive adsorption of PAHs onto graphene-based materials. SEM, TEM and FTIR provided evidence for the adsorption of PAHs and successful regeneration of the adsorbent accompanied by distinct morphological changes. Isotherm experiments revealed that adsorption of PAHs was significantly influenced by hydrophobic interactions between the sorbate and hydrophobic surface of GW. The Freundlich multilayer isotherm model best fit the experimental data obtained for both multi-component PAH and single-solute experiments as indicated by the Error Sum of Squares (SSE) obtained from nonlinear regression analysis. Experiments revealed that competitive adsorption had a limiting effect on the overall adsorption capacity as $q_{\max}$ and K_d were higher in single-solute than multi-component PAH experiments. The results suggest that partition distribution coefficients *(K_d)* between the solid-liquid interphase played a significant role in the overall adsorption and a positive correlation between K_d and LogK_{ow} of PAHs was established in single-solute experiments. Sorption-desorption experiments revealed that PAHs were adsorbed with a maximum removal efficiency of 100 % at an optimum GW dosage of 2 g/L. Adsorption thermodynamics revealed that PAH adsorption onto GW is spontaneous and endothermic. The adsorbent was regenerated and reused for up to six times and its efficiency remained fairly constant.

Keywords: *Polycyclic aromatic hydrocarbons; Graphene wool; Competitive sorption; Decontamination, Aqueous solution*.

1 Introduction

Polycyclic aromatic hydrocarbons (PAHs) are a ubiquitous and toxic class of xenobiotic organic contaminants composed of carbon and hydrogen; with proven carcinogenicity such as skin, lung and bladder cancer [1]. They are released into the environment via incomplete combustion, forest fires, burning of fuels, oil spills, urban run-off and other anthropogenic activities [2,3]. PAHs are inadvertently found in food, air, soil, sediment, drinking water and other water bodies [4,5]. Thus the need for a sustainable, efficient and cost-effective remediation approach cannot be over-emphasized.

Graphene has attracted immense global attention from researchers due its structural tunability, thermodynamic stability and well-defined physicochemical properties [6]. Recent developments arising from studies related to graphene has brought about promising applications, ranging from biomedicine, nano-sensors, super-capacitors, pollution monitoring, control and remediation [7-14]. In the field of environmental science, graphene-based materials have been harnessed as efficient next-generation sorbents for water purification applications because their surfaces are largely hydrophobic, porous, and they possess high adsorption affinities for a vast number of organic contaminants (OCs) [15].

The graphene wool (GW) used in this study was synthesized via a chemical deposition method using quartz wool as a substrate, under optimized flow rates of hydrogen, argon and methane gas as precursors [16]. The adsorption and desorption of phenanthrene and pyrene onto this wool-like graphene adsorbent have been reported based on single-solute, batch sorption experiments [13]. The sorption kinetics were found to follow a pseudo-second order reaction pathway and 24 hours was suitable for optimum adsorption. Furthermore, because single-solute experiments were conducted, several sorption models were easily fitted to isotherm data and a multilayer adsorption

mechanism was described via Freundlich and Sips models with $R^2 > 0.99$, and removal efficiencies for individual PAH was > 98 %.

However, PAHs are a large class of organic compounds which are rarely found as single solutes in real-life polluted samples [17,18]. Therefore, to establish the actual robustness and efficiency of this novel graphene wool in the decontamination of field water samples, it is necessary to carry out multi-solute, competitive adsorption experiments and account for optimum adsorbent dosage under multi-solute contamination conditions. Furthermore, information regarding the adsorption of 15 co-existing PAHs onto any absorbent is not available in literature, which makes it almost impossible to fully understand the adsorptive behaviour of the PAH class of pollutants in a multi-solute environment.

Therefore, the aim of this study was to evaluate the sorption mechanism controlling the interaction between graphene wool and selected polycyclic aromatic hydrocarbons in aqueous solution via single-solute and multi-component (PAH mix) batch experiments. Furthermore, effects of temperature (adsorption thermodynamics) and adsorbent dosage were determined, as well as removal efficiency from graphene wool (GW) wherein several cycles of regeneration and re-use were evaluated.

2 Materials and Method

2.1. Materials

9-30 µm coarse quartz wool (Arcos Organics, New Jersey, USA), argon and hydrogen (99.999%, Afrox, South Africa), calcium chloride, sodium azide, hexane and acetone (98 % purity, Sigma-Aldrich, Germany) were purchased. A QTM PAH mix and internal standard (Sigma-Aldrich, USA), were used for PAH mix adsorption experiments. The mixed standard contained 2000 mg/L of 15 EPA priority polycyclic aromatic hydrocarbons [19], prepared in dichloromethane

(naphthalene, acenaphthene, acenaphthylene, fluorene, phenanthrene, anthracene, fluoranthene, pyrene, benzo(a)anthracene, chrysene, benzo(b)fluoranthene, benzo(a)pyrene, indeno (1,2,3-cd)pyrene, dibenz(a,h)anthracene and benzo(g,h,i) perylene); and the internal standard used was mixture of d8-naphthalene, d10-phenathrene, d10-pyrene and d12-chrysene. Neat standards of naphthalene, anthracene, benzo(a)anthracene, benzo(a)pyrene and benzo(ghi)perylene respectively (99% purity) were purchased from Supelco (USA) for use in single-solute batch experiments. Polytetrafluoroethylene (PTFE) membrane syringe filters (0.22 µm and 0.45 µm) were purchased from Stargate Scientific (South Africa). Reversed phase C_{18} solid phase extraction (SPE) cartridges were purchased from CNW Technologies (Shanghai, China). All the solutions were prepared with ultra-pure water obtained from a Milli-Q water (9.2 µS/cm^3) purification system (Millipore, Bedford, MA, USA).

2.2. Adsorbent

Graphene wool was synthesized by a chemical vapour deposition (CVD) method using the optimum established procedure [16]. The quartz wool was placed in a horizontal quartz tube, with the prescribed flow rate of argon, hydrogen and methane gas released at specified time intervals and at an elevated temperature of 1200 ºC. The graphene wool was characterized by high resolution transmission electron microscopy (TEM) using a JEOL JEM 2100F (JOEL Ltd, Tokyo, Japan) operated at 200 kV; scanning electron microscopy was also carried out with the aid of Zeiss Ultra Plus 55 field emission scanning electron microscope (FE-SEM), operated at 2.0 kV (Zeiss, Germany); Fourier transformed infrared spectroscopy (FTIR) was carried out using a Bruker Alpha-T spectrometer (Bruker Optik GmbH, Ettlingen, Germany), whilst the specific surface area was determined using Sear's method. Refer to [13,16] for a detailed description of the GW

synthesis and characterization thereof by various means including high-resolution X-ray photoelectron spectroscopy (XPS) and Raman spectroscopy.

2.3. Sorption isotherm experiments

Batch adsorption experiments of the PAH mixture and single-solute/single PAHs by graphene wool (GW) were performed in 40 mL PTFE screw capped amber vials (Stargate Scientific, South Africa) sealed with aluminum foil at 25 ± 1 °C. Background solution (pH = 7.0) contained 0.01 mol/L $CaCl_2$ (ACE, South Africa) in deionized water with 200 mg/L NaN_3 (Sigma-Aldrich, Germany) as a biocide. Table 1 provides a list of the PAHs used as sorbates in this study and their properties. The isotherm experiment was conducted with initial concentrations of the PAH mix and single PAH solutions, ranging from 2 µg/20 mL to 10 µg/20 mL obtained by serial dilution with deionized water and 1 % methanol to ensure solubilization of PAHs in aqueous medium [20]. The adsorption of the PAH mix and individual PAHs onto graphene wool was carried out in batch experiments using a thermostated shaking water bath (Wisebath, Celsius Scientific, South Africa). To investigate the effect of initial concentration of the solution, 20 mg of GW was introduced into 5 vials containing 2, 4, 6, 8 and 10 µg /20 mL of PAH mixture and individual PAHs, respectively. Each concentration was tested in triplicate. Desorption experiments were carried out as previously described [21]; immediately after the adsorption studies, the supernatant was completely removed and 20 mL of 0.01 mol/L $CaCl_2$ containing 200 mg/L of sodium azide was added to the solid residue. The amount of PAH recovered in solution was determined after equilibration for 24 h and at 25 ºC. To determine the effect of adsorbent dosage, adsorption experiments were carried out using varying adsorbent masses (20, 25, 30 and 50 mg), for PAH mix concentrations of both 400 and 500 µg/L, in order to determine the average removal efficiencies per dosage. For all the batch experiments, suspensions were agitated at 200 rpm in a shaking water bath for 24 h at 25 ºC, based

on previous reports [13,22], and subsequently centrifuged at 9860 x g for 20 min to recover a clear supernatant solution.

2.4. Quantification

Prior to determination of the equilibrium concentration (C_e) for single-solute sorption experiments, the vials were centrifuged at 9860 x g for 20 min and 2 mL aliquots of the supernatants were filtered through 0.45 μm syringe filters. Equilibrium concentrations of naphthalene (NAPH), anthracene (ANT), benzo(a)anthracene (B(a)ANT), benzo(a)pyrene (B(a)p)) and benzo(ghi)perylene (PERY) were determined using a Horiba Jobin Yvon Fluoromax-4 spectrofluorometer (Horiba instruments Inc., Edison, NJ, USA) at excitation wavelengths of 280, 300, 320, 330 and 420 nm respectively, with calibration equations derived from 0.2 μg/20 mL to 10 μg/20 mL concentrations of individual PAHs [13].

Solid phase extraction (SPE) was carried with the aid of preconditioned C_{18} SPE cartridges (CNW Technologies, China) for multi-solute adsorption experiments, prior to GC-MS analysis [23]. The supernatant was loaded on the cartridge and washed with 5 mL of methanol/deionized water (50:50). The analytes were eluted with 6 mL hexane using the SPE vacuum pump at a flow rate of 0.5 $mLmin^{-1}$. The eluate recovered was concentrated by reducing its volume to 1 mL under nitrogen flow. A matrix-matched calibration was obtained by spiking 20 mL blank deionized water with 2, 4, 6, 8 and 10 μg/20 mL of PAH mix and carrying out the same SPE extraction explained above (equivalent to 2, 4, 6, 8 and 10 ng of PAH mix injected into the GC column in triplicate) and the resulting calibration line equation was used to calculate the equilibrium concentration (C_e). The concentration of PAHs not adsorbed after agitating the solution for 24 h with GW was determined using gas chromatography (GC, Agilent 6890) hyphenated with mass spectrometry

(MSD, Agilent 5975C). The amount of PAHs adsorbed (C_s) was determined by the difference between the initial and equilibrium liquid-phase concentrations (C_e) (eq. 1 and 2). Each experiment was repeated three times.

$$C_s = \frac{(C_0 - C_e)V_0}{S_m} \quad (1)$$

$$\text{Removal efficiency (\%)} = \frac{(C_0 - C_e)}{C_0} \times 100 \quad (2)$$

Where C_o (mg/L) is the initial concentration, C_e (mg/L) is the equilibrium solute concentration, V_o is the initial volume (L) and S_m is the mass (g) of the adsorbent.

Graphene wool was regenerated by rinsing with 10 mL hexane and a mixture of acetone-water (50:50) respectively using a thermostated shaker for 2 hr successively at room temperature. Afterwards, the GW was dried in a muffle furnace (Labotec, South Africa) at a temperature of 70 ˚C for 4 hr and was allowed to cool before re-use.

2.5. GC-MS Instrumentation

PAH analysis for multi-solute adsorption experiments was carried out with the aid of a gas chromatograph (GC, Agilent 6890) hyphenated to a mass spectrometer (MSD, Agilent 5975C) in electron impact ionization mode. The analytes (1 µL splitless injection) were separated on a Restek Rxi-PAH column with the following dimensions: 60 m long, 0.25 mm internal diameter and 0.10 µm film thickness. Helium gas of purity > 99 % (Afrox, Gauteng) was used as carrier gas in constant flow mode at 1 mL/min. The inlet temperature was at 275 ºC and the GC oven temperature was held at 80 ºC for 1 min, then ramped at 30 ºC/min to 180 ºC, and subsequently to 320 ºC at 5 ºC/min. The run-time for each injection was 75 min. The ionization potential was 70 eV, the source temperature was 230 ºC and the quadrupole was at 150 ºC. A mass range of m/z 40-350 was

recorded in full scan mode. For better sensitivity, the selective ion monitoring mode was employed to detect and quantify the PAH analytes [24]. The 0.5 ng/µL pure PAH mix standard (Sigma-Aldrich, USA) which had been dissolved in hexane was injected to determine the retention time and mass spectrum of each PAH (Figure 1). The internal standard used was a mixture of d8-naphthalene, d10-phenathrene, d10-pyrene and d12-chrysene (0.5 ng/µL). Quantification of the selected PAHs was carried out using five-point calibration curves with concentrations ranging from 2 µg/20 mL to 10 µg/20 mL for all PAHs used in this study. The calibration was derived from the plot of the target analyte peak area divided by the peak area of the internal standard versus the concentration of analyte.

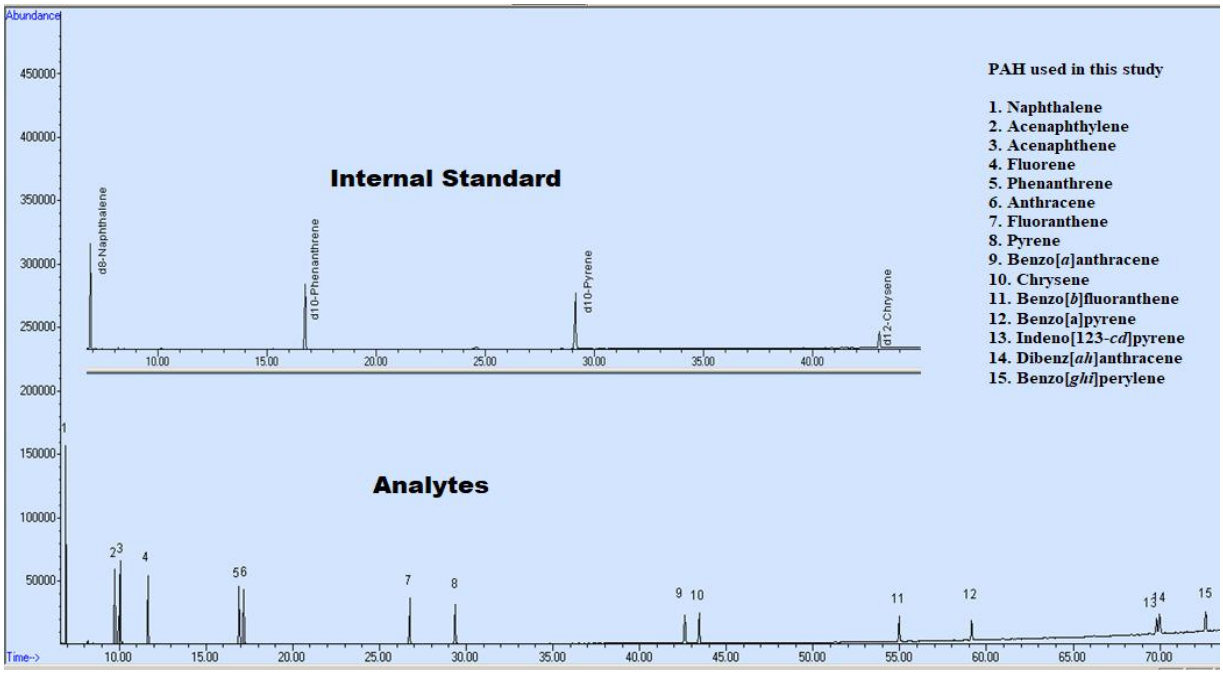

Figure 1: Representative GC-MS SIM chromatogram of the PAH standard mixture after SPE extraction of 10 µg/20 mL PAH aqueous solution. The IS mixture contained d8-naphthalene, d10-phenanthrene, d10-pyrene, d12-chrysene in hexane.

Table 1: Physicochemical properties of the 15 target polycyclic aromatic hydrocarbons.

PAHs	**[a] Molecular formula**	**[ab] Boiling point (ºC)**	**[ac] Log K_{ow}**	**[a] S_w (mg/L)**	**[a] M_w (g/mol)**
Naphthalene	$C_{10}H_8$	217.9	3.30	31.00	128.17
Acenaphthene	$C_{12}H_{10}$	279.0	3.92	3.90	154.21
Acenaphthylene	$C_{12}H_8$	280.0	3.94	9.00	152.19
Fluorene	$C_{13}H_{10}$	294.0	4.18	1.69	166.22
Phenanthrene	$C_{14}H_{10}$	338.4	4.46	1.10	178.23
Anthracene	$C_{14}H_{10}$	341.3	4.45	1.29	178.23
Fluoranthene	$C_{16}H_{10}$	384.0	5.16	0.26	202.25
Pyrene	$C_{16}H_{10}$	394.0	4.88	0.14	202.25
Benzo(a)anthracene	$C_{18}H_{12}$	437.6	5.76	9.4e-3	228.30
Chrysene	$C_{18}H_{12}$	448.0	5.81	2.0e-3	228.30
Benzo(b)fluoranthene	$C_{20}H_{12}$	481.0	6.12	1.5e-3	252.30
Benzo(a)pyrene	$C_{20}H_{12}$	496.0	6.13	1.62e-3	252.30
Indeno(1,2,3-cd)pyrene	$C_{22}H_{12}$	536.0	6.58	6.9e-4	276.30
Dibenz(a,h)anthracene	$C_{22}H_{14}$	524.0	6.50	5e-4	278.30
Benzo(g,h,i)perylene	$C_{22}H_{12}$	550.0	6.63	2.6e-4	276.30

B_p: boiling point (ºC) [b] [25,26], Log K_{ow}: octanol–water partition coefficient [c] [27], S_w: water solubility (mg/L), M_w: molecular weight (g/mol) [a] [28].

3 Results and Discussion

3.1 Sorbent characterization

Comprehensive information regarding the characterization of this novel material is available in the literature [13,16]. In addition, the pH of GW was found to be 6.1 and 7.1 in $CaCl_{2(aq)}$ solution and deionized water respectively. The specific surface area of GW, as determined using Sear's method, is 279 m^2/g, which is lower than the theoretical specific surface area of graphene (2630 m^2/g) due to coverage over the quartz wool which ultimately defines the specific surface area [29,30]. The morphology of the adsorbent in its pristine state, after adsorption of PAHs and regeneration were examined using scanning electron microscopy and transmission electron microscopy (SEM & TEM) (Figure 2). The high-resolution microscopic analysis revealed that the diameter of each strand of graphene wool is between 6 - 8 microns. Figure 2 (a & d) revealed extensive coverage of quartz wool by graphene with a heterogenous and rough surface structure, while Figure 2 (b, c & e) revealed obvious morphological changes as a result of the adsorption and regeneration processes. Furthermore, Fourier transformed infrared spectroscopy (Figure 2f) revealed two prominent peaks; one peak associated with the sp^2 hybridized C=C backbone of graphene at 775 cm^{-1}, and a broad peak at 1059 cm^{-1} associated with Si-O-C arising from the functionalized quartz wool (SiO_2) coated with graphene [31]. The doublet peak at 2925 and 2845 cm^{-1} is attributed to symmetric and asymmetric sp^2 and sp^3 C-H stretching bands, whilst the peak at 675 cm^{-1} is attributed to C-H out-of-plane bending vibrations of aromatic rings [32]

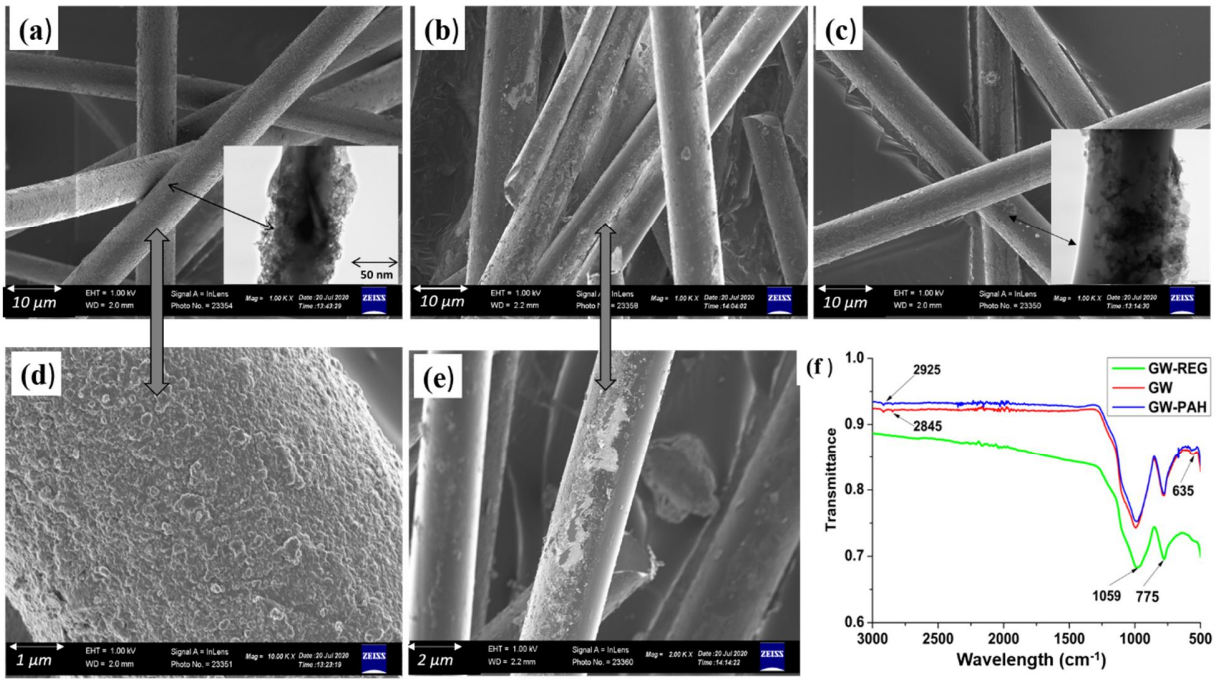

Figure 2: (a) SEM image of pristine graphene wool (1000x) {Inset: TEM image of pristine GW}; (b) SEM image of graphene wool after PAH mix adsorption (1000x); (c) SEM image of regenerated graphene wool (1000x) {Inset: TEM image of regenerated graphene wool}; (d) SEM image of pristine graphene wool (10,000x); (e) SEM image of GW post-adsorption (2000x); (f) FTIR of pristine GW, GW after PAH adsorption (GW-PAH) and regeneration (GW-REG).

3.2 Adsorption isotherm

Adsorption isotherm studies provide vital information on the interaction between sorbates and sorbents, especially the amount of analyte adsorbed, and the amount left in solution after equilibrium is reached [33]. Linear regression (eq. 5) and nonlinear isotherm models such as Freundlich (eq. 3) and Langmuir models (eq. 4) were used to fit adsorption experimental data. The Error Sum of Squares (SSE) (eq. 7) was used to test models used in this study.

$$q_e = K_f C_e^N \qquad (3)$$

$$q_e = \frac{q_{max} K_L C_e}{1 + K_L C_e} \qquad (4)$$

$$q_e = K_d C_e \qquad (5)$$

$$R_L = \frac{1}{1+K_L q_{max} C_0} \quad (6)$$

$$\sum_{i=1}^{n} (q_{e,cal} - q_{e,exp})_i^2 \quad (7)$$

where K_f (μg/g) (L/μg)^N) and N (dimensionless) are the Freundlich constant and intensity parameter, an indicator of site energy heterogeneity; q_{max} (μg/g) and K_L (L/μg) are the Langmuir maximum adsorption capacity and Langmuir constant associated with solute–surface interaction energy, respectively; q_e is the solid-phase concentration (μg/g), C_e is the liquid phase equilibrium concentration (μg/L), and K_d (L/g) is the sorption distribution coefficient [22,34]. The value of the separation factor R_L (eq. 6) provides important information about the nature of adsorption. The value of R_L is between 0 and 1 for favourable adsorption, while $R_L>1$ represents unfavourable adsorption and $R_L = 1$ represents linear adsorption. The adsorption process is irreversible if $R_L = 0$ [35,36]

The isotherm parameters obtained for the PAH mix (multi-solute) adsorption by GW revealed that the Freundlich isotherm model, which reflects a multilayer adsorption mechanism, best fit experimental data compared to the uniform site energy and monolayer sorption mechanism described by the Langmuir model. This was validated by values of SSE presented in Table 2 [34]. The Langmuir model only fit at lower equilibrium concentrations, but as the concentration increased, the adsorption pattern deviated as a result of site saturation towards a multilayer adsorption pattern. The R_L values for all the PAHs were greater than zero and less than 1, which depicts favourable adsorption [34,37]. The core adsorption mechanism for the interaction between mixtures of PAHs and GW is mainly controlled by $\pi - \pi$ non-covalent bonding and hydrophobic interactions, however, other adsorption mechanisms centered around molecular conformation of

the adsorbent and adsorbate also play a role in the multi-solute adsorption of PAHs [30]. The SEM images in Figure 2 confirm that mass transfer occurred between the boundary layer of PAH contaminated water and GW, leading to adsorption of the sorbate onto the active sites (pore walls and holes) of GW. The largely rough and heterogeneous surface of the wool-like material aided the adsorption of the PAHs by increasing the available surface area. The irregular pattern in the values obtained and reported in Table 2 is mainly as a result of the highly competitive nature of the adsorption processes, due to the number of PAH molecules competing for available sites simultaneously.

Table 2: Sorption isotherm parameters for multi-component PAH adsorption by graphene wool (GW) and Error Sum of Squares (SSE) of non-linear regression analysis (Experimental conditions: GW dosage = 20 mg per 20 mL; mixing rate = 200 rpm; T = 25 ± 1 °C; Initial conc.: 2 µg/20 mL – 10 µg/20 mL; contact time = 24 hours).

PAHs	**Freundlich**			**Langmuir**				**Linear**		***Amount adsorbed***
	K_f	***SSE***	***N***	q_{max} ***(µg/g)***	***SSE***	K_L ***(L/µg)***	R_L	K_d ***(L/g)***	***SSE***	***(µg/g)***
Naphthalene	2.5e-5	2.36	2.85	1.63e3	2.37	2.0e-4	9.10e-1	0.22	2.67	155
Acenaphthene	1.2e-1	4.98	0.66	4.47e2	4.99	6.7e-5	9.90e-1	0.03	4.98	156
Acenaphthylene	3.6e-1	4.00	5.40	7.90e-1	4.42	7.2e3	2.76e-7	-0.07	4.44	185
Fluorene	3.4e-1	4.00	5.40	9.40e-1	4.71	5.7e1	3.52e-5	-0.08	4.73	176
Phenanthrene	2.8e-5	4.12	2.69	1.27e3	4.23	1.2e-4	9.43e-1	0.15	4.23	126
Anthracene	1.7e-5	1.03	3.19	1.81e3	1.20	4.5e-4	8.17e-1	-0.02	4.99	164
Fluoranthene	1.5e-5	0.76	3.32	3.71e3	1.00	2.8e-4	8.78e-1	-0.08	4.78	175
Pyrene	1.6e-5	0.64	3.29	3.16e3	0.95	3.3e-4	8.59e-1	-0.08	4.79	173
Benzo(a)anthracene	2.2e-5	1.19	3.13	1.01e2	1.30	6.1e-1	3.27e-3	-0.03	4.98	166
Chrysene	4.0e-5	0.78	3.05	2.96e2	1.00	2.9e-4	8.69e-1	0.03	4.99	161
Benzo(b)fluoranthene	3.6e-3	0.59	2.14	5.65e2	0.78	1.7e-4	9.23e-1	-0.07	4.82	161
Benzo(a)pyrene	1.6e-1	0.71	1.24	6.45e2	0.74	1.4e-4	9.37e-1	-0.06	4.88	152
Indeno(1,2,3-cd)pyrene	1.1e-4	1.85	2.77	8.87e1	1.89	6.2e-1	3.23e-3	-0.04	3.97	192
Dibenz(a,h)anthracene	7.8e-5	1.81	2.86	9.09e1	1.87	6.0e-1	3.30e-3	-0.04	3.96	193
Benzo(g,h,i)perylene	3.2e-5	2.02	3.27	4.91e3	2.13	3.8e-4	8.39e-1	-0.13	3.31	225

3.3 Single-solute adsorption isotherms of selected PAHs

Sorption of naphthalene (NAPH), anthracene (ANT), benzo(a)anthracene (B(a)ANT), benzo(a)pyrene (B(a)P) and benzo(g,h,i)perylene (PERY) onto graphene wool (GW) were studied individually in a batch isotherm experiments. Similar process variables as the PAH mixture/multi-solute adsorption experiment were maintained for better comparison {viz. adsorbent dosage (1 g/L); individual PAH initial concentration (C_o = 2 to 10 µg/20 mL); time (24 hr); pH (7); temperature (25 °C); and rpm (200)}.

The Freundlich multilayer adsorption mechanism best described the sorption experimental data for the selected 2-6 ringed PAHs, as this model provided the lowest Error Sum of Squares (SSE) (Table 3). The adsorption capacity (K_d) and predicted amount adsorbed (q_e) were higher for higher molecular weight (HMW) PAHs than for lower molecular weight (LMW) PAHs (Table 3, Figure 3). This suggests that adsorption of PAHs onto GW is influenced by the hydrophobicity of the compounds (Figure 4). However, the maximum holding or adsorption capacity (q_{max}), Freundlich adsorption capacity (K_f) and adsorption capacity (K_d) were significantly higher for the selected 2-6 ringed PAHs than those reported in Table 2. This affirms that competitive adsorption in a multi-solute aqueous medium had a limiting effect on the overall sorption of the PAHs by graphene wool.

Table 3: Freundlich, Langmuir and linear sorption parameters for single-solute adsorption of selected 2-6 ringed PAHs onto GW.

Sorption model	Parameter	NAPH	ANT	B(a)ANT	B(a)P	PERY
	K_f	9.35	9.88e-3	5.61	54.47	5.51e-4
Freundlich	*N*	0.27	2.34	0.58	1.05	6.03
	SSE	0.39	0.88	0.12	1.43	0.68
Langmuir	q_{max} *(µg/g)*	4.89e1	1.22e4	2.35e3	1.52e3	1.60e4
	K_L *(L/µg)*	2.52e-2	1.56e-4	5.94e-3	8.73e3	7.87e-4
	SSE	0.44	1.52	0.13	1.47	1.36
Linear	K_d *(g/L)*	0.17	1.92	3.62	5.73	12.50
	Predicted q_e *(µg/g)*	66.63	189.53	202.390.17	336.25	432.00
	SSE	0.77	1.51	0.48	1.43	1.36

Freundlich model: $q_e = K_f C^N e$*; Langmuir model,* $q_e = q_{max} Ce/(K_L + C_e)$*; Linear model:* $q_e = K_d C_e$ *; Exp.* q_e*: Predicted amount adsorbed; SSE: Error Sum of Squares.*

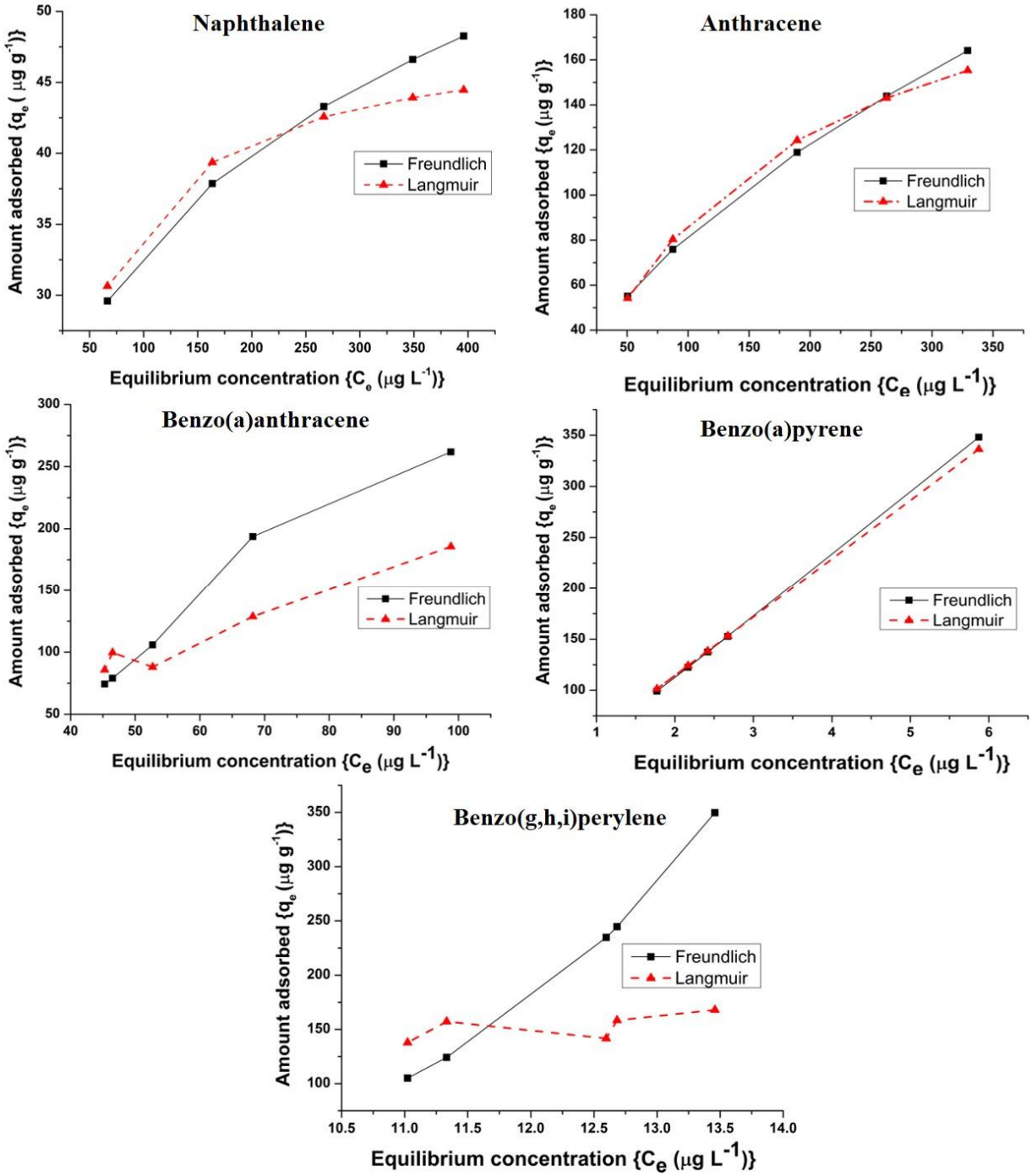

Figure 2: Representation of the Freundlich and Langmuir isotherm models for adsorption of selected individual 2-6 ringed PAHs onto graphene wool using nonlinear regression analysis.

3.4 Influence of hydrophobicity on competitive adsorption of PAHs

The trend in adsorption of the PAH mixture onto GW can also be elucidated by the effect of hydrophobicity of the PAHs in solution, which can be determined from the logarithm of the octanol/water partition coefficient (LogK_{ow}) [38,39]. There is positive trend in the molecular mass of the compounds and the octanol/water partition coefficients, however, there are PAHs with the same molecular mass but with a slight difference in the value of Log$K_{ow,}$ which is as a result of their molecular conformation or structure [40,41].

Table 3 and Figure 4 reveal that K_d increased with increase in the LogK_{ow} of the PAHs adsorbed by GW in single-solute experiments, similar to what was previously reported by Lamichhanne *et al*. [42] for acenaphthene, fluorene, phenanthrene, fluoranthene, and pyrene adsorption by different organic carbon fractions. The correlation between sorption capacity and LogK_{ow} is due the fact that water molecules surround the hydrophobic compounds to form a cage-like structure which stabilizes the less soluble or more hydrophobic PAHs in aqueous solution [43]. The binding mechanism for the PAH molecules onto GW is believed to be dominated by van der Waals-type interactions, also known as hydrophobic bonding [37]. Therefore, the PAH molecules that are more hydrophobic with higher values of LogK_{ow}, favourably interact with GW with stronger hydrophobic interactions and adsorption capacity (K_{ads}) than the less hydrophobic PAHs. This is similar to what was reported by Li *et al*. [44] via DFT simulations of graphene interaction with PAHs, and interaction of a mesoporous silica-based adsorbent with benzo(b)fluoranthene, benzo(a)pyrene, and benzo(g,h,i)perylene [45].

However, there is an obvious deviation from the trend shown in the adsorption of a multi-component PAH mixture, as the correlation between Log K_{ow} and K_d decreased due to the expected complex chemistry of the solution. It is also noteworthy that competitive interaction led to a

significant decrease in the adsorption capacity of GW for the respective PAHs (Figure 4). Hydrophobicity and $\pi - \pi$ electron interactions should have favoured sorption of high molecular weight (HMW) and more hydrophobic PAHs in the multi-solute experiment, however, Figure 4 reveals otherwise. This suggests that other factors such as size of the molecules, molecular dynamics/conformations and surface structure of the adsorbent (pore volume & size) may have enhanced adsorption of low molecular weight (LMW) PAHs in the competitive adsorption process.

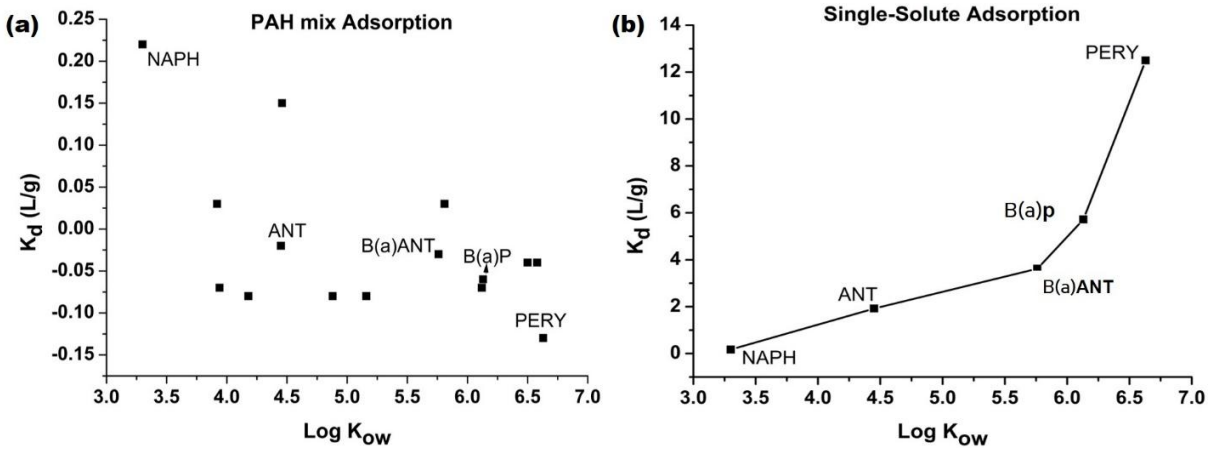

Figure 4: Correlation between hydrophobicity (Log*Kow*) and adsorption capacity (K_d) of PAH interactions with graphene wool at 25˚C, (a) adsorption of PAH mixture (unlabelled data points represent other PAHs present in the mix) (b) single-solute adsorption of selected PAHs.

3.5 Effect of adsorbent dosage

The adsorbent dose of 20, 25, 30 and 40 mg was added to 20 mL solutions containing 8 µg/20 mL and 10 µg/20 mL of PAHs, to determine the average removal efficiency with varying sorbent mass, while other parameters viz. time (24 hr), pH (7), temperature (25 °C) and rpm (200) constant. With increase in the dosage, PAH removal efficiency increased. The average removal efficiency ranged from 52.2 – 72.6 % at 20 mg, 55.1 – 80 % at 25 mg, 65.3 – 85.1 % at 30 mg and 80 – 100 % at 40

mg dosage, respectively (Figure 5). The results also revealed that competitive adsorption of higher molecular weight (HMW) PAHs were favoured over lower molecular weight (LMW) PAHs, and the improvement in the removal efficiency can be attributed to the availability of vacant sites as dosage increased. Further increase in the adsorbent dosage would potentially yield improvement in removal of LMW PAHs, as HMW PAH removal efficiency already reached its optimum at 40 mg/20 mL (2 g/L) for both 8 µg/20 mL and 10 µg/20 mL PAH concentrations.

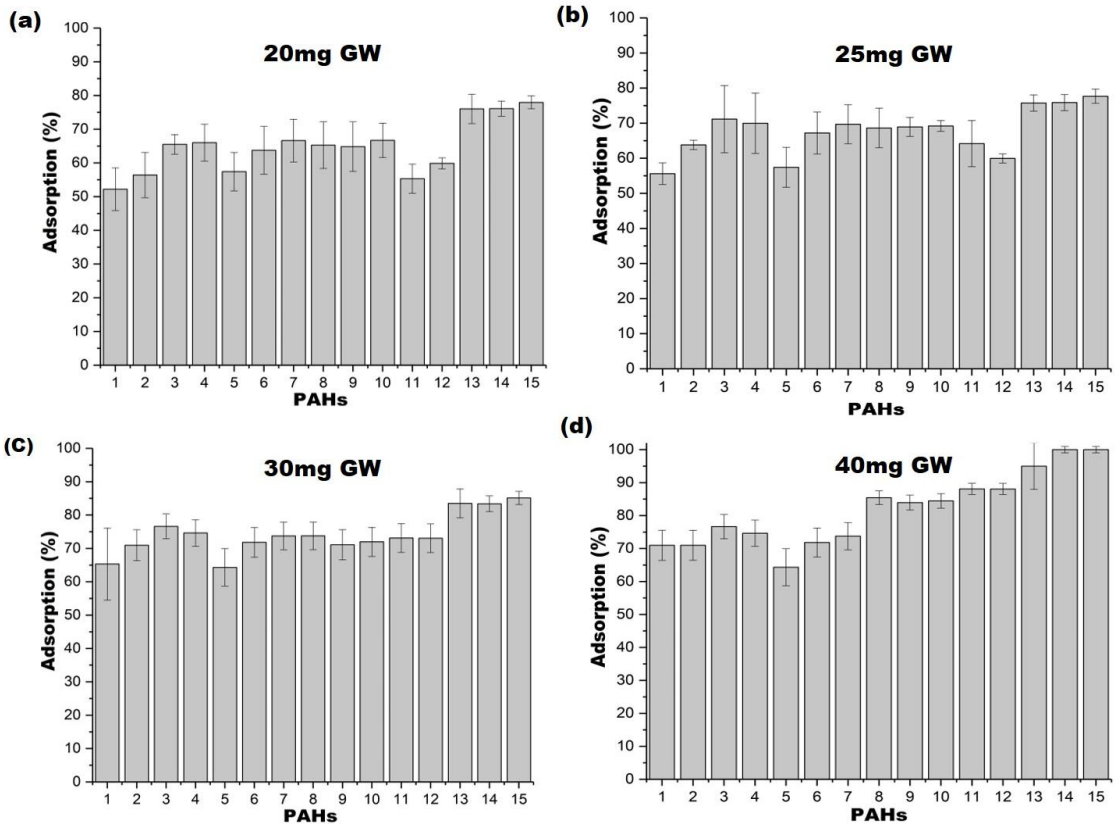

Figure 5: Effect of increasing dose of graphene wool (GW) in 20 mL of 400 µg/L and 500 µg/L PAH solution (a) 20 mg GW (b) 25 mg GW (c) 30 mg GW (d) 40 mg GW; (Experimental conditions: 25ºC, 200 rpm mixing rate, n= 3). PAHs are; 1= Naphthalene, 2= Acenaphthene, 3= Acenaphthylene, 3= Fluorene, 4= Phenanthrene, 4= Anthracene, 5= Fluoranthene, 6= Pyrene, 7= Benzo(a)anthracene, 8= Chrysene, 9= Benzo(b)fluoranthene, 10= Benzo(a)pyrene, 11= Indeno(1,2,3-cd)pyrene, 12= Dibenz(a,h)anthracene, 13= Benzo(g,h,i)perylene, 14= Dibenz(a,h)anthracene, 15= Benzo(g,h,i)perylene.

3.6 Desorption experiment and hysteresis

The Freundlich constant "*N*" which is regarded as the heterogeneity index and *H*-index which represent the hysteresis index (reversibility of the sorption process) [36] are presented in Table 4. The *N* value for adsorption (N_{ads}) and *H*-indices were generally higher in multi-solute sorption than for single-solute experiments. The trend in heterogeneity presented is expected due to the number of solutes interacting simultaneously with GW, thus resulting in a more heterogenous sorption-desorption process. Figure 6 revealed that a significant amount of PAHs adsorbed were desorbed with % desorption ranging 45 to 75 % for PAH mix experiments, while the reverse is the case for in the single-solute experiments as desorption was found to decrease, ranging from 5.5 to 56.4 %. Furthermore, the trend observed in single-solute desorption in Figure 6 suggests stronger binding interactions between HMW PAHs and GW, supported by the adsorption capacities (K_d) obtained (Table 3); leading to significant sorption irreversibility. It has been reported that lower ring PAHs are preferentially bound to sorbent active sites at lower concentrations and partitioning favours adsorption of higher ring PAHs as concentration increases in a multi-solute, competitive environment [37,39]. Generally, given the high percentage of adsorbed species that were desorbed into aqueous solution in the PAH mix adsorption, it can be inferred that a significant amount of PAHs were loosely held by weak van der Waal forces and π–π interactions [46], due to significant competition for sorption sites and saturation thereof, and Table 2 also reported lower binding capacity for the PAH mix.

Furthermore, reports revealed that the percent desorption of PAHs in single solute environments are somewhat different from what is obtained for a multi-component systems using geosorbents rich in carbon, and it was suggested that the presence of less hydrophobic PAHs improved the solubility of more hydrophobic solutes, thus increasing their percentage desorption [21]. However,

such an effect was absent in the single-solute experiments. Evaluation of Table 4 reveals that higher molecular weight compounds displayed more hysteretic sorption behavior with higher *H*-indices. This is expected as stronger $\pi - \pi$ interaction with GW is expected between higher ring PAHs than lower ring PAHs due to the number of π electrons, thus making irreversible entrapment or slow desorption more evident with higher ring PAHs. This result correlates with hydrophobicity of the PAHs, the higher the value of LogK_{ow}, the more recalcitrant the PAHs are towards desorbing into aqueous medium [47,48]. Pore-deformation of adsorbents may occur during the sorption process leading to entrapment of PAHs and/or slow desorption rates, which is more likely in multi-solute sorption-desorption processes, leading to higher *H*-indices [49].

Table 4: Comparison of sorption-desorption parameters and hysteresis index (H) of selected PAHs in multi-solute (M) and single-solute (S) interactions with graphene wool (GW)

PAH	$K_{f\ (des)}$ **(M)**	$K_{f\ (des)}$ **(S)**	$N_{(ads)}$ **(M)**	$N_{(ads)}$ **(S)**	$N_{(des)}$ **(M)**	$N_{(des)}$ **(S)**	***H*** **(M)**	***H*** **(S)**
Naphthalene	2.28	271.58	2.85	0.27	0.80	0.96	**3.56**	**0.28**
Anthracene	2.23	7.25	3.19	2.34	0.30	4.37	**10.63**	**0.54**
Benzo(a)anthracene	1.73	314.60	3.13	0.58	0.29	1.05	**10.79**	**0.55**
Benzo(a)pyrene	1.91	134.75	1.34	1.05	0.17	0.70	**7.88**	**1.50**
Benzo(g,h,i)perylene	1.75	1.35	3.27	6.03	0.30	1.75	**10.9**	**3.45**

*$N_{(ads)}$: Freundlich adsorption intensity, $N_{(des)}$: Freundlich desorption intensity; **H**: Sorption–desorption hysteresis index, $H=N_{ads}/N_{des}$; **M:** PAH mixture; **S:** Single-solute.*

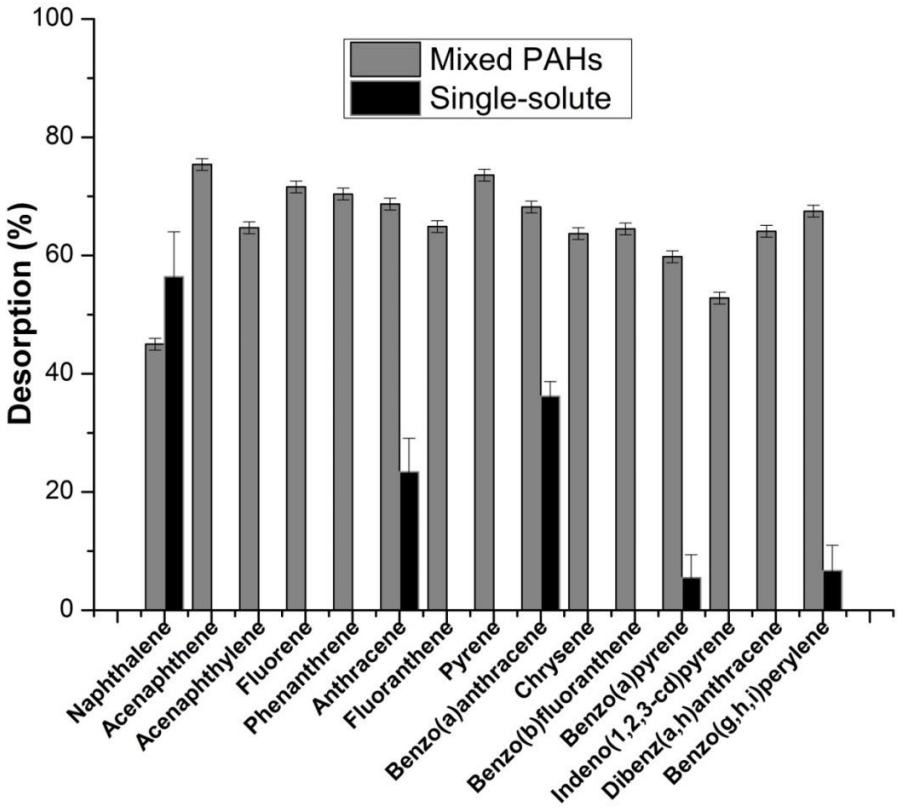

Figure 6: Average desorption rate (%) of PAHs recovered in aqueous solution (Experimental conditions: 20 mL of de-ionized water; temperature: 25 ˚C). Error bars show ± standard deviation, n= 3.

3.7 Regeneration and reusability experiment

Graphene wool (GW) was regenerated with n-hexane. Six successive cycles of adsorption experiments were carried out with a PAH concentration range of 2 µg/20 mL to 10 µg/20 mL. The removal efficiency of the PAHs from the GW after each regeneration cycle is shown in Figure 7. The regeneration procedure proved efficient as the removal efficiency of the material was relatively constant, suggesting multiple reusability of the material for remediation of water contaminated with several PAHs simultaneously. However, there is indication that small fragments of the GW were lost during the regeneration cycles, as around 9.6 % loss in total mass of the adsorbent was recorded over the entire cycle of six regeneration steps. Morphological changes as

a result of the regeneration process after 6 cycles was examined with the aid of TEM, SEM and FTIR, and it revealed that layers of adsorbed solute, appearing as patches on the surface of the adsorbent, were desorbed or removed to a large extent by the regeneration process (Figure 2 c & d). However, TEM revealed some degree of loss of coverage (Inset: Figure 2 (a & c) and FTIR showed a decline in peak intensities (Figure 2f)). This loss was potentially responsible for the slight decline in removal efficiency observed for the higher molecular weight PAHs. On the contrary, the removal efficiency of the lower mass PAHs seemed to improve, which suggests that the surface of material may have undergone a slight deformation which may have favoured smaller sized molecules [47,48].

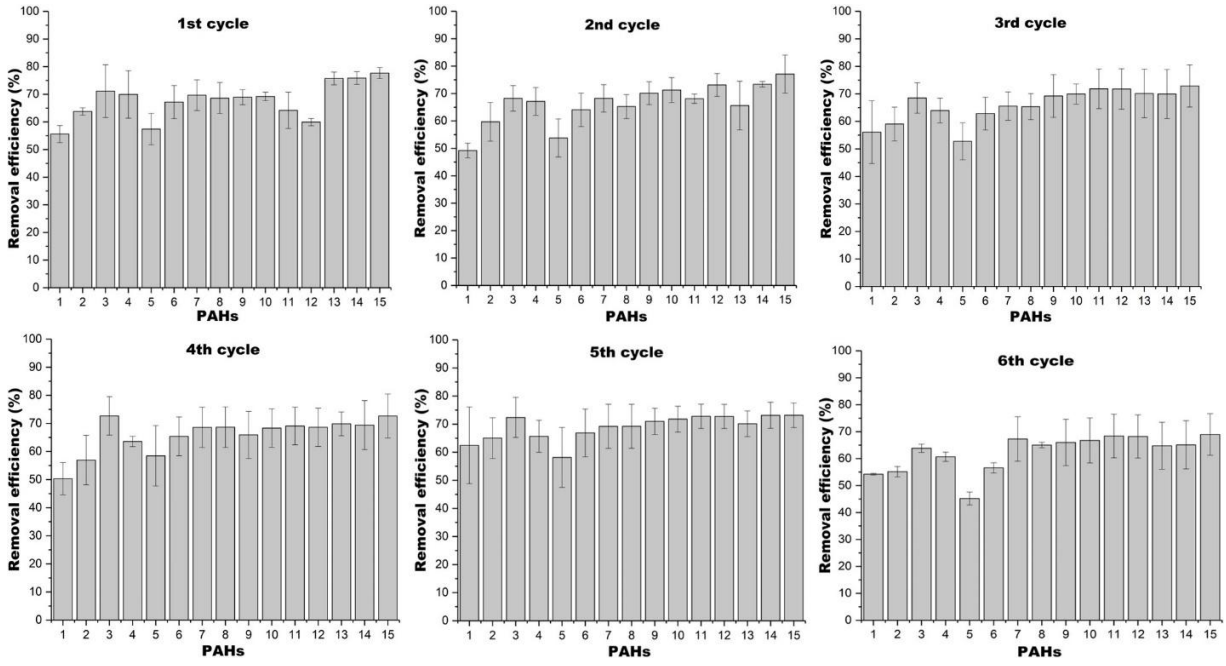

Figure 7: Percentage adsorption of the PAHs used in this study by GW (Experimental conditions- mass of adsorbent: 20 mg; volume of solution: 20 mL; temperature: 25˚C, concentration of PAHs: 2 µg/20 mL to 10 µg/20 mL). Error bars show ± standard deviation, n= 3. PAHs are; 1= Naphthalene, 2= Acenaphthene, 3= Acenaphthylene, 3= Fluorene, 4= Phenanthrene, 4= Anthracene, 5= Fluoranthene, 6= Pyrene, 7= Benzo(a)anthracene, 8= Chrysene, 9= Benzo(b)fluoranthene, 10= Benzo(a)pyrene, 11= Indeno(1,2,3-cd)pyrene, 12= Dibenz(a,h)anthracene, 13= Benzo(g,h,i)perylene, 14= Dibenz(a,h)anthracene, 15= Benzo(g,h,i)perylene.

3.8. Adsorption thermodynamics of selected 2 - 6 ringed PAHs

Adsorption is temperature dependent whereby some processes are feasible at ambient temperature while others require an additional supply of heat energy to overcome an energy barrier or initiate a reaction. The effect of temperature on the adsorption of NAPH, ANT, B(a)ANT, B(a)P and PERY onto graphene wool (GW) was studied at 298, 308 and 318 K, respectively. The adsorption data was fit to a linear isotherm model (eq. 5), and it was observed that the equilibrium concentration of the selected PAHs reduced and adsorption capacity (K_d) increased with increase in temperature, except for NAPH which is likely due to volatilization losses (Table 5). Thermodynamic parameters such as Gibbs free energy change (ΔG˚), enthalpy (ΔH˚) and entropy (ΔS˚) were calculated using the Van't Hoff equations (eqs. 8 and 9), in order to elucidate the nature of adsorption of NAPH, ANT, B(a)ANT, B(a)P and PERY onto GW as a function of temperature [13,50].

$$\ln K_d = \frac{\Delta S^\circ}{R} - \frac{\Delta H^\circ}{RT} \quad (8)$$

$$\Delta G^\circ = -RT ln\, K_d \quad (9)$$

where ΔG is the change in the Gibbs free energy (kJ/mol); ΔH is the change in enthalpy (kJ/mol), and ΔS is the change in entropy (kJ/mol), R = gas constant (8.314 J/mol K), T = thermodynamic temperature (K), and K_d = adsorption capacity (L/g).

Table 5 revealed that adsorption of selected PAHs onto GW involved a spontaneous endothermic reaction, with positive and negative values of ΔH and ΔG respectively, except for NAPH. Furthermore, an increase in temperature improved the sorption feasibility of ANT, B(a)ANT, B(a)P and PERY, considering the trend in ΔG values. The low enthalpy values (ΔH) suggest that PAH interaction with GW is mainly physisorption and not chemisorption [50]. Several reports have shown that the thermodynamic behavior of PAHs differ with respect to interactions

with different adsorbents [13,42,45,50,51]. However, there is a consensus that thermodynamic parameters are mostly influenced by the morphology of the sorbent and physicochemical properties of the sorbate. The information provided in this study reveals the vital role of temperature regimes towards the potential application of GW for removal of PAHs from aqueous solution.

Table 5: Thermodynamic parameters for adsorption of selected 2 – 6 ringed PAHs onto graphene wool (GW)

PAHs	**Temperature (K)**	K_d *(L/g)*	**ΔG°** *(kJ/mol)*	**ΔH°** *(kJ/mol)*	**ΔS°** *(kJ/mol K)*
Naphthalene	308	0.17	4540	-8.81e-2	1.41e-2
	318	0.15	4858		
	328	0.14	5198		
Anthracene	308	1.92	-1616	3.06e-2	4.74e-2
	318	1.94	-1657		
	328	1.99	-1818		
Benzo(a)anthracene	308	0.65	-1067	8.31e-4	2.83e-2
	318	1.59	-1188		
	328	2.20	-2085		
Benzo(a)pyrene	308	5.73	-6268	1.66e-4	2.83e-2
	318	6.58	-6587		
	328	12.07	-6958		
Benzo(g,h,i)perylene	308	12.50	-10030	2.49e-5	2.82e-2
	318	12.70	-10721		
	328	13.90	-12673		

3.9. Comparison with previous studies

Researchers have reported on the competitive adsorption of PAHs onto different adsorbents. Activated carbon was used to adsorb 15 PAHs from vegetable oil and 68-93 % efficiency was

achieved with the recalcitrant higher molecular weight PAHs having better removal efficiency [51]. The removal of fluorene, pyrene, benzo(k)fluoranthene, benzo(a)pyrene and benzo(g,h,i)perylene from water using immature coal (leonardite) was studied [52]. The results showed that adsorption increased with increase in LogK_{ow} and adsorption efficiency of 82 % was recorded for B[*a*]P and B[*k*]F.

Competitive adsorption of phenanthrene, pyrene, fluorene, fluoranthene and benzo(a)anthracene onto zeolite and organo-zeolite have been reported [53]. Results showed that adsorption indices were in the range of 50-83% for organo-zeolite and less than 50 % for zeolite, with the exception of benzo(a)anthracene which recorded the highest removal efficiency of 75 % due to its higher partition coefficient (log K_{ow}). Wang et al. [30] reported that adsorption of selected PAHs on graphene nanosheets and graphene oxide increased with increase in hydrophobicity in the order pyrene > phenanthrene > naphthalene. A more recent report involving zeolite and modified zeolite as adsorbents recorded the following removal efficiencies for PAHs; 47.6 and 43.9 % for the zeolite and modified zeolite for benzo(k)fluoranthene, 62.9 and 69.5 % for benzo(b)fluoranthene, and 43.8 and 37.2 % for benzo(a)pyrene [45]. Most of the values were less than what was recorded for graphene wool, nonetheless, they also reflect the dominant influence of hydrophobicity on the overall uptake of PAHs in a competitive and multi-solute environment.

4 Conclusion

This study revealed that a mixture of several polycyclic aromatic hydrocarbons categorized as priority pollutants by the United States Environmental Protection Agency can be effectively removed from water using a novel graphene wool as adsorbent. The robust, flexible and porous nature of this material makes it a suitable adsorbent for the simultaneous adsorption of PAHs. Sorption-desorption studies revealed that higher molecular weight PAHs were better removed by

the GW. The release potential into aqueous medium was also evaluated and results indicated the occurrence of hysteresis (some degree of irreversible adsorption). The optimum dosage was 2 g/L (40 mg/20 mL) of GW adsorbent for higher molecular weight PAHs, with concentration as high as 10 µg/20 mL and average removal efficiencies at optimum dosage were between 71 to 100 % with good RSDs values (1 – 5.5 %, n = 3). Hydrophobic and $\pi - \pi$ interactions dominated the adsorption process of the PAHs investigated in this study in the single-solute experiments, whilst molecular size/conformation of PAHs, morphology of adsorbent and solution chemistry influenced multi-solute competitive adsorption. Results obtained from the regeneration and reusability experiments showed that GW was reasonably stable and can be reused without significant loss of efficiency. With the right fabrication, this new form of graphene (GW) may be used to make filters and adsorbents for water purification purposes due to its wool-like structure, water permeability and other morphological and physicochemical properties. The material can also be harnessed for the decontamination of water containing other emerging hydrophobic pollutants, as a result of its proven affinity for hydrophobic organic contaminants such as PAHs.

Acknowledgements

Authors are grateful to University of Pretoria Commonwealth Doctoral Scholarship, Departments of Chemistry and Physics at the University of Pretoria, especially Prof. Ncholu Manyala, Dr. Liezel Van der Merwe, Genna-Leigh Schoonraad, Chiedza Munyeza and Sifiso Nsibande.

Conflict of interest

The authors declare that there is no conflict of interest regarding the publication of this article.

Identifiers

Adedapo O. Adeola: *orcid.org/0000-0002-7011-2396*

Patricia B.C. Forbes: *orcid.org/0000-0003-3453-9162*

https://www.researchgate.net/profile/Patricia_Forbes

References

1. Cai S.-S., Syage J. A., Hanold K. A., Balogh M. P. UltraPerformance liquid chromatography−atmospheric pressure photoionization-tandem mass spectrometry for high-sensitivity and high-throughput analysis of U.S. Environmental Protection Agency 16 priority pollutants polynuclear aromatic hydrocarbons. *Analytical Chemistry*, 2009; **81**(6), 2123-8. https://doi.org/10.1021/ac802275e
2. Olivella M. A., Ribalta T. G., de Febrer A. R., Mollet J. M., de las Heras F. X. C. Distribution of polycyclic aromatic hydrocarbons in riverine waters after Mediterranean forest fires. *Science of The Total Environment*, 2006; **355**(1), 156-66. https://doi.org/10.1016/j.scitotenv.2005.02.033
3. Karyab H., Yunesian M., Nasseri S., Mahvi A. H., Ahmadkhaniha R., Rastkari N. Nabizadeh R. Polycyclic Aromatic Hydrocarbons in drinking water of Tehran, Iran. *Journal of Environmental health science & engineering*, 2013; **11**(1), 25-32. https://doi.org/10.1186/2052-336X-11-25
4. Maliszewska-Kordybach B., Smreczak B. & Klimkowicz-Pawlas A. Concentrations, sources, and spatial distribution of individual polycyclic aromatic hydrocarbons (PAHs) in agricultural soils in the Eastern part of the EU: Poland as a case study. *Science of The Total Environment*, 2009; **407**(12), 3746-53. https://doi.org/10.1016/j.scitotenv.2009.01.010
5. Martorell I., Perelló G., Martí-Cid R., Castell V., Llobet J. M., Domingo J. L. Polycyclic aromatic hydrocarbons (PAH) in foods and estimated PAH intake by the population of

Catalonia, Spain: Temporal trend. *Environment International*, 2013; **36**(5), 424-432. https://doi.org/10.1016/j.envint.2010.03.003

6. Kyzas G. Z., Deliyanni E. A., Bikiaris D. N., Mitropoulos A. C. Graphene composites as dye adsorbents: Review. *Chemical Engineering Research and Design*, 2018; **129**, 75-88. https://doi.org/10.1016/j.cherd.2017.11.006
7. Li X., Wang X., Zhang L., Lee S., Dai H. Chemically derived, ultrasmooth graphene nanoribbon semiconductors. *Science*, 2008b; **319**(5867), 1229-32. https://doi.org/10.1126/science.1150878
8. Vermeir M., Lachau-Durand S., Mannens G., Cuyckens F., van Hoof B., Raoof A. Absorption, metabolism, and excretion of darunavir, a new protease inhibitor, administered alone and with low-dose ritonavir in healthy subjects. *Drug Metabolism and Disposition*, 2009; **37**(4), 809. https://doi.org/10.1124/dmd.108.024109
9. Mueller T., Xia F. N., Avouris P. Graphene photodetectors for high-speed optical communications. *Nature Photonics*, 2010; **4,** 297– 301. https://doi.org/10.1038/nphoton.2010.40
10. Zhang L., Xia J., Zhao Q., Liu L., Zhang Z. Functional graphene oxide as a nanocarrier for controlled loading and targeted delivery of mixed anticancer drugs. *Small*, 2010; **6**(4), 537-44. https://doi.org/10.1002/smll.200901680
11. Hu M., Mi B. Enabling graphene oxide nanosheets as water separation membranes. *Environmental Science & Technology*, 2013; **47**(8), 3715-3723. https://doi.org/10.1021/es400571g

12. Paixão M. M., Vianna M. T. G., Marques M. Graphene and graphene nanocomposites for the removal of aromatic organic compounds from the water: systematic review. *Materials Research Express,* 2018; **5**(1), 012002. https://doi.org/10.1088/2053-1591/aaa047
13. Adeola A. O., Forbes P. B. C. Optimisation of the sorption of selected polycyclic aromatic hydrocarbons by regenerable graphene wool. *Water Science and Technology*, 2019; 80(10), 1931-1943. https://doi.org/10.2166/wst.2020.011
14. Nsibande S. A., Forbes P. B. C. Development of a turn-on graphene quantum dot-based fluorescent probe for sensing of pyrene in water. *RSC Advances,* 2020; **10**, 12119-12128. https://doi.org/10.1039/C9RA10153E
15. Ersan G., Apul O. G., Perreault F., Karanfil T. Adsorption of organic contaminants by graphene nanosheets: A review. *Water Research*, 2017; **126**, 385-98. https://doi.org/10.1016/j.watres.2017.08.010
16. Schoonraad G.-L., Madito M. J., Manyala N., Forbes P. Synthesis and optimisation of a novel graphene wool material by atmospheric pressure chemical vapour deposition. *Journal of Materials Science*, 2020; **55**, 545-64. https://doi.org/10.1007/s10853-019-03948-0
17. Abdel-Shafy, H. I., Mansour, M. S. M. A review on polycyclic aromatic hydrocarbons: Source, environmental impact, effect on human health and remediation. *Egyptian Journal of Petroleum*, 2016; **25**, 107-123. https://doi.org/10.1016/j.ejpe.2015.03.011
18. Mojiri A., Zhou J. L., Ohashi A., Ozaki N., Kindaichi T. Comprehensive review of polycyclic aromatic hydrocarbons in water sources, their effects and treatments. *Science of The Total Environment*, 2019; 696, 133971, 1-16. https://doi.org/10.1016/j.scitotenv.2019.133971
19. USEPA, U.S. Environmental Protection Agency office of the science advisor risk assessment forum. *Framework for human health risk assessment to inform decision making*. 2014.

https://www.epa.gov/sites/production/files/2014-12/documents/hhra-framework-final-2014. (accessed 23 February 2020).

20. Crisafully R., Milhome M. A., Cavalcante R. M., Silveira E. R., De Keukeleire D., Nascimento R. F. Removal of some polycyclic aromatic hydrocarbons from petrochemical wastewater using low-cost adsorbents of natural origin. *Bioresources Technology*, 2008; **99**(10), 4515-9. https://doi.org/10.1016/j.biortech.2007.08.041
21. Hussein T. A. & Ismail Z. Z. Desorption of selected PAHs as individuals and as a ternary PAH mixture within a water-soil-nonionic surfactant system. *Environmental Technology*, 2013; **34**(3), 351-61. https://doi.org/10.1080/09593330.2012.696718
22. Vidal C.B., Barros A.L., Moura C.P., de Lima A.C.A., Dias F.S., Vasconcellos L.C.G., Fechine P. B.A., Nascimento R.F. Adsorption of polycyclic aromatic hydrocarbons from aqueous solutions by modified periodic mesoporous organosilica. *Journal of Colloid and Interface Science*, 2011; **357**(2), 466-73. http://doi.org/10.1016/j.jcis.2011.02.013
23. Sibiya P., Potgieter M., Cukrowska E., Jönsson J. A., Chimuka L. Development and application of solid phase extraction method for polycyclic aromatic hydrocarbons in water samples in Johannesburg area, South Africa. *South African Journal of Chemistry*, 2012; **65**, 206–213.
24. Munyeza C. F., Dikale O., Rohwer E. R., Forbes P. B. C. Development and optimization of a plunger assisted solvent extraction method for polycyclic aromatic hydrocarbons sampled onto multi-channel silicone rubber traps. *Journal of Chromatography* A, 2018; 1555, 20-9. https://doi.org/10.1016/j.chroma.2018.04.053

25. May W. E., Wasik S. P., Freeman D. H. Determination of the solubility behavior of some polycyclic aromatic hydrocarbons in water. *Analytical Chemistry,* 1978; **50**(7), 997-1000. https://doi.org/10.1021/ac50029a042

26. Haynes W. M. CRC Handbook of Chemistry and Physics, 2009−2010, 90th ed. *Journal of the American Chemical Society*, 2009*;* 131, 12862-12862. https://doi.org/10.1021/ja906434c

27. Hansch C., Leo A., Hoekman D. *Exploring QSAR - hydrophobic, electronic, and steric constants*. Washington, DC: American Chemical Society, 1996; 39, 1189-1190. https://doi.org/10.1021/jm950902o

28. Kim S., Chen J., Cheng T., Gindulyte A., He J., He S., Li Q., Shoemaker B. A., Thiessen P. A., Yu B., Zaslavsky L., Zhang J., Bolton E. E. PubChem 2019 update: improved access to chemical data. *Nucleic Acids Research*, 2018, **47**(D1), D1102-D9. https://dx.doi.org/10.1093%2Fnar%2Fgky1033

29. Stoller M.D., Park S., Zhu Y., An J., Ruoff R.S. Graphene-based ultracapacitors. *Nano Letters*, 2018; **8**(10), 3498-502. https://doi.org/10.1021/nl802558y

30. Wang J., Chen Z., Chen B. Adsorption of polycyclic aromatic hydrocarbons by graphene and graphene oxide nanosheets. *Environmental Science & Technology,* 2014; **48**(9), 4817-25. https://doi.org/10.1021/es405227u

31. Ţucureanu V., Matei A, Avram A.M. FTIR spectroscopy for carbon family study. *Critical Reviews in Analytical Chemistry*, 2016, 46, 502-520. https://doi.org/10.1080/10408347.2016.1157013

32. Yang H., Li F., Shan C., Han D., Zhang Q, Niu L., Ivaska A. Covalent functionalization of chemically converted graphene sheets via silane and its reinforcement. *Journal of Materials Chemistry*, 2009, 19, 4632-4638. https://doi.org/10.1039/B901421G

33. Cooney D. O. Adsorption Designer for Wasterwater Treatment. 1999; Lewis, Boca Raton, Fl. : Lewis Publishers, London, England.
34. Anthony E.T., Ojemaye M.O., Okoh A.I., Okoh O.O. Synthesis of CeO_2 as promising adsorbent for the management of free-DNA harboring antibiotic resistance genes from tap-water, *Chemical Engineering Journal*, 2020, 401, 125562. https://doi.org/10.1016/j.cej.2020.125562
35. Rahman M. S., Islam M. R. Effects of pH on isotherms modeling for Cu (II) ions adsorption using maple wood sawdust. *Chemical Engineering Journal*, 2009; 149, 273–80. https://doi.org/10.1016/j.cej.2008.11.029
36. Ololade I. A., Adeola A. O., Oladoja N. A., Ololade O. O., Nwaolisa S. U., Alabi A. B. Ogungbe I. V. In-situ modification of soil organic matter towards adsorption and desorption of phenol and its chlorinated derivatives. *Journal of Environmental Chemical Engineering*, 2018; **6**(2), 3485-3494. https://doi.org/10.1016/j.jece.2018.05.034
37. Wang X., Sato T., Xing B. Competitive sorption of pyrene on wood chars. *Environmental Science & Technology*, 2006; **40**(10), 3267-72. https://doi.org/10.1021/es0521977
38. Li L., Xie S., Cai H., Bai X., Xue Z. Quantitative structure-property relationships for octanol-water partition coefficients of polybrominated diphenyl ethers. *Chemosphere*, 2008a; **72**(10), 1602-6. https://doi.org/10.1016/j.chemosphere.2008.04.020
39. Zou M., Zhang J., Chen J., Li X. Simulating adsorption of organic pollutants on finite (8,0) single-walled carbon nanotubes in water. *Environmental Science & Technology*, 2012; **46**(16), 8887-94. https://doi.org/10.1021/es301370f

40. Sabljić A., Güsten H., Verhaar H., Hermens J. QSAR modelling of soil sorption. improvements and systematics of log KOC vs. log KOW correlations. *Chemosphere*, 1995, **31**(11), 4489-514. https://doi.org/10.1016/0045-6535(95)00327-5
41. Toropov A. A., Toropova A. P., Raska I. QSPR modeling of octanol/water partition coefficient for vitamins by optimal descriptors calculated with SMILES. *European Journal of Medicinal Chemistry*, 2008; **43**(4), 714-40. https://doi.org/10.1016/j.ejmech.2007.05.007
42. Lamichhane S., Bal Krishna K. C., Sarukkalige R. Polycyclic aromatic hydrocarbons (PAHs) removal by sorption: a review. *Chemosphere* 2016; 148, 336-53. https://doi.org/10.1016/j.chemosphere.2016.01.036
43. Atkins P., Paula J. Physical Chemistry for the Life Sciences. 2006; W. H. Freeman and Company, New York.
44. Li B., Ou P., Wei Y., Zhang X., Song J. Polycyclic aromatic hydrocarbons adsorption onto graphene: a DFT and AIMD study. *Materials (Basel, Switzerland)*, 2018, **11**(5), 726. https://doi.org/10.3390/ma11050726
45. Costa J. A. S., de Jesus R. A., da Silva C. M. P., Romão L. P. C. Efficient adsorption of a mixture of polycyclic aromatic hydrocarbons (PAHs) by Si–MCM–41 mesoporous molecular sieve. *Powder Technology*, 2017; **308**, 434-41. https://doi.org/10.1016/j.powtec.2016.12.035
46. Okoli C. P., Adewuyi G. O., Zhang Q., Zhu G., Wang C., Guo Q. Aqueous scavenging of polycyclic aromatic hydrocarbons using epichlorohydrin, 1,6-hexamethylene diisocyanate and 4,4-methylene diphenyl diisocyanate modified starch: Pollution remediation approach. *Arabian Journal of Chemistry*, 2015; **12**(8), 2760-2773. https://doi.org/10.1016/j.arabjc.2015.06.004

47. Nguyen T. H., Sabbah I., Ball W. P. Sorption nonlinearity for organic contaminants with diesel soot: method development and isotherm interpretation. *Environmental Science & Technology,* 2004; **38**(13), 3595-603. https://doi.org/10.1021/es0499748
48. Sander M., Pignatello J.J. Sorption irreversibility of 1,4-dichlorobenzene in two natural organic matter–rich geosorbents. *Environmental Toxicology and Chemistry*, 2009; **28**(3), 447-57. https://doi.org/10.1897/08-128.1
49. Jonker M.T. O., Koelmans, A. A. Extraction of polycyclic aromatic hydrocarbons from soot and sediment: solvent evaluation and smplications for sorption mechanism. *Environmental Science & Technology*, 2002; **36**, 4107-4113. https://doi.org/10.1021/es0103290
50. Yakout M., Daifullah A.A.M. Removal of selected polycyclic aromatic hydrocarbons from aqueous solution onto various adsorbent materials, *Desalination and Water Treatment*, 2013, 51, 6711-6718. https://doi.org/10.1080/19443994.2013.769916
51. Gong Z., Alef K., Wilke B.-M. Li P. Activated carbon adsorption of PAHs from vegetable oil used in soil remediation. *Journal of Hazardous Materials*, 2007; **143**(1), 372-8. https://doi.org/10.1016/j.jhazmat.2006.09.037
52. Zeledón-Toruño Z. C., Lao-Luque C., de las Heras F. X. C. Sole-Sardans M. Removal of PAHs from water using an immature coal (leonardite). *Chemosphere,* 2007; **67**(3), 505-12. https://doi.org/10.1016/j.chemosphere.2006.09.047
53. Lemić J., Tomašević-Čanović M., Adamović M., Kovačević D., Milićević S. Competitive adsorption of polycyclic aromatic hydrocarbons on organo-zeolites. *Microporous and Mesoporous Materials,* 2007; **105**(3), 317-323. https://doi.org/10.1016/j.micromeso.2007.04.014